

Construction of Multifunctional Fe₃O₄-MTX@HBc Nanoparticles for MR Imaging and Photothermal Therapy/Chemotherapy

Qiang Zhang^{2*}, Wenjun Shan^{1*}, Chaochao Ai¹, Zhiwei Chen³, Tiantian Zhou³, Xiaolin Lv¹, Xi Zhou¹, Shefang Ye¹, Lei Ren^{1, 4, 5}  and Xiumin Wang² 

1. Key Laboratory of Biomedical Engineering of Fujian Province University/Research Center of Biomedical Engineering of Xiamen, Department of Biomaterials, College of Materials, Xiamen University, Xiamen 361005, Fujian, P. R. China.
2. School of Pharmaceutical Sciences, Xiamen University, Xiamen 361002, Fujian, P. R. China.
3. Department of Electronic Science, Fujian Provincial Key Laboratory of Plasma and Magnetic Resonance Research, Xiamen University, Xiamen 361005, Fujian, P. R. China.
4. Fujian Collaborative Innovation Center for Exploitation and Utilization of Marine Biological Resources, Xiamen University, Xiamen 361005, Fujian, P. R. China.
5. State Key Lab of Physical Chemistry of Solid Surfaces, Xiamen University, Xiamen 361005, P. R. China.

*These authors contributed equally to this work.

 Corresponding authors: Lei Ren, Key Laboratory of Biomedical Engineering of Fujian Province University/Research Center of Biomedical Engineering of Xiamen, Department of Biomaterials, College of Materials, Xiamen University, Xiamen 361005, P. R. China. Email: renlei@xmu.edu.cn; Xiumin Wang, School of Pharmaceutical Science, Xiamen University, Xiamen 361002, P. R. China. Email: wangxm@xmu.edu.cn.

© Ivyspring International Publisher. This is an open access article distributed under the terms of the Creative Commons Attribution (CC BY-NC) license (<https://creativecommons.org/licenses/by-nc/4.0/>). See <http://ivyspring.com/terms> for full terms and conditions.

Received: 2017.07.16; Accepted: 2017.11.10; Published: 2018.01.01

Abstract

To accomplish effective cancer imaging and integrated therapy, the multifunctional nanotheranostic Fe₃O₄-MTX@HBc core-shell nanoparticles (NPs) were designed. A straightforward method was demonstrated for efficient encapsulation of magnetic NPs into the engineered virus-like particles (VLPs) through the affinity of histidine tags for the methotrexate (MTX)-Ni²⁺ chelate. HBc₁₄₄-His VLPs shell could protect Fe₃O₄-MTX NPs from the recognition by the reticuloendothelial system as well as could increase their cellular uptake efficiency. Through our well-designed tactic, the photothermal efficiency of Fe₃O₄ NPs were obviously improved *in vitro* and *in vivo* upon near-infrared (NIR) laser irradiation. Moreover, Magnetic resonance imaging (MRI) results showed that the Fe₃O₄-MTX@HBc core-shell NPs were reliable T₂-type MRI contrast agents for tumor imaging. Hence the Fe₃O₄-MTX@HBc core-shell NPs may act as a promising theranostic platform for multimodal cancer treatment.

Key words: Virus-Like Nanoparticles; MRI; Chemotherapy; Photothermal Therapy; Theranostic

Introduction

Chemotherapy is one of the major categories of the medical discipline specifically devoted to pharmacotherapy for cancer. However, the current chemotherapeutic agents have many adverse effects on healthy tissues or normal cells.¹ Continuing improvement in the tumor specific multifunctional nanoparticles for targeting and efficient delivery of drugs to tumor cells is an area of intense research with the potential to revolutionize the treatment of cancer.^{2,3} Recently, the combination of photothermal and chemotherapy is widely applied in killing cancer

cells by using nanoparticles, such as nanosized graphene oxide,⁴ gold nano particles,⁵ plasmonic copper sulfide nanocrystals,⁶ folate-lipid-poly(lactico-glycolic acid) lipid-polymer nanoparticles⁷ and so on.

As a major class of nanoparticles, magnetic nanoparticles have been examined extensively for applications in cancer therapy due to their ultra-small size, biocompatibility and magnetic properties.^{8,9} More recently, clustered Fe₃O₄ magnetic nanoparticles have been reported to possess broad optical

absorption in the near-infrared (NIR) range and have further been used as a class of photosensitizers for tumor photothermal therapy (PTT).¹⁰ Compared with other photosensitive nanomaterials, Fe₃O₄ nanoparticles possess various advantages, such as: 1) superior biocompatibility; 2) biodegradability (Fe₃O₄ nanoparticles can be degraded into iron ions *in vivo* and excess iron ions can be transferred into ferritin proteins for iron storage and detoxification), and 3) good superparamagnetic properties make them as excellent contrast agents for magnetic resonance imaging (MRI).^{11,12} However, due to the easy agglomeration and the limited functional groups of Fe₃O₄ nanoparticles, a suitable material coating, such as silica, polyethylene glycol (PEG), bovine serum albumin (BSA) and so on, is always necessary to improve the situations and is of significance for bioapplications.¹³⁻¹⁵

Lately, virus-like particles have attracted much attentions because of their potential to be a new drug delivery system for clinical therapy.¹⁶ The VLPs are multimeric protein assemblies that can serve as robust synthetic carriers due to the ability to encase nucleic acids or other small molecules by self-assembling in proper conditions.¹⁷ The protein shells of VLPs are steady to protect the cargos from quick releasing in blood circulation and can be chemically and genetically readily modified by genetic engineering or chemical methods.¹⁸ The size of VLPs are commonly between 18 - 100 nm in diameter, makes them easily internalized by cells and biodegradable with extremely low cytotoxicity. The VLPs exhibit the potential to be a safe drug delivering system.¹⁹ VLP-based core-shell nanoparticles have been widely applied in biomedical applications. For example, Zhang Y. et al. have prepared quantum dots (QDs) loaded HIV-1 based lentivirus for tracking virus infection.²⁰ Fang PY. et al. have encapsulated functional RNAs into bacteriophage Q β VLPs to attenuate cell proliferation and promote mortality of brain tumor cells.²¹ Moreover, Li C. et al. have constructed Ag₂S QDs loaded simian virus 40 VLPs for real-time *in vivo* NIR-II imaging.²² However, the integrated single function of the developed VLPs based core-shell nanoparticles limited their efficacy for tumor imaging and therapy. Therefore, it is vital to develop multifunctional VLPs based nanoprobe for tumor imaging and therapy.

The hepatitis B virus core antigen (HBc) could spontaneously assemble into an icosahedral particle in all viable prokaryotic and eukaryotic recombinant expression systems.²³ Herein, we designed and developed a novel magnetic drug delivery system (Fe₃O₄-MTX@HBc), in which MTX was chemically conjugated to Fe₃O₄ nanoparticles and subsequently

embedded into a shell of hepatitis B virus core protein (HBc) VLPs. As a natural nanocarrier, HBc presented empty interior space that can enhance the stability and biocompatibility of the nanodrugs. Moreover, the HBc VLPs can be easily modified with functional groups using the methods of genetic or chemical engineering.²⁴⁻²⁶ Owing to these merits, HBc VLPs can be a promising candidate as nanocarriers.

The detailed synthetic procedures and potential applications for this drug delivery system were illustrated in Scheme 1. The multifunctional Fe₃O₄-MTX NPs still hold the photothermal and magnetic properties after modified MTX on the surface. The viral nature and the essence of protein of HBc₁₄₄-His VLPs could facilitate the internalization of Fe₃O₄-MTX by the cancer cells. The presence of VLPs shell could also provide a protective layer for drug molecules and magnetite nanoparticles from the recognition by the reticuloendothelial system, therefore allowing drugs to be administered over prolonged periods.

Materials and Methods

Materials

Ferric chloride (FeCl₃), anhydrous sodium acetate (NaOAc), and hexahydrate nickel chloride (NiCl₂·6H₂O) were purchased from Shantou Xilong Chemical Factory (Guangdong, China). Dimercaptosuccinic acid (DMSA), phosphotungstic acid (TPA), dicyclohexyl carbodiimide (DCC) and MTX were purchased from Sigma-Aldrich (ST. Louis, USA), N-hydroxysuccinimide (NHS) were purchased from Solarbio (Beijing, China). Diethylene glycol (DEG), glycerol, and dimethyl sulfoxide (DMSO) were purchased from Sinopharm Chemical Reagent Co. Ltd. (Shanghai, China). Urea, glycine, tris(hydroxymethyl) aminomethane (Tris), 3-(4,5-dimethylthiazol-2-yl)-2,5-diphenyltetrazolium bromide (MTT) and Annexin V-FITC/PI Apoptosis Detection Kit were purchased from KeyGen Biotech Co. Ltd. (Nanjing, China). RPMI 1640 culture medium and penicillin-streptomycin were purchased from Biological Industries (Beit Ahemeq, Israel). Fetal bovine serum (FBS) and trypsin were purchased from Invitrogen (California, USA). All chemicals were used without further purification. Ultrapure water (18.2 M Ω cm) were obtained from Milli-Q Water Purification System.

Preparation and characterization of Fe₃O₄ and Fe₃O₄-MTX@HBc

Synthesis of Fe₃O₄-MTX-Ni²⁺ nanocomposites

Fe₃O₄ NPs were prepared according to a former literature method.²⁷ DMSA modified Fe₃O₄ NPs

(11.7±1.6 nm in diameter) were obtained by the procedure as previously described.²⁸ 240 mg of the as-prepared Fe₃O₄-DMSA NPs were firstly re-dispersed in 20 ml of DMSO. 400 mg of DCC and 400 mg of NHS were then added and stirred for 30 min before magnetic separation. 24 mg of MTX and 24 ml of DMSO were added to the precipitation and stirred for 12 h before magnetic separation. The addition of DCC and NHS to the Fe₃O₄-DMSA could form a highly reactive intermediate (NHS-carboxylate), which could subsequently react with the free amino group on MTX.²⁹ The supernatant was collected to determine unloaded MTX and subsequently to calculate the drug loading efficiency (% , w/w). Afterwards, Fe₃O₄-MTX-Ni²⁺ complexes were acquired by mixing 23 mg of Fe₃O₄-MTX NPs with 240 mg of NiCl₂ (0.1 M aqueous solution) for 30 min and finally extracted by magnetic separation.

Preparation of Fe₃O₄-MTX@HBc NPs

HBc₁₄₄-His VLPs were prepared following the method from our former research with minor modifications²⁸. In brief, HBc₁₄₄-His VLPs were produced by *Escherichia coli* expression system and purified by ion-exchange column chromatography and molecular sieve chromatography. Herein, 23 mg of HBc₁₄₄-His VLPs were disassembled after incubating with 15 ml of the denaturant stock solution (2.5 M urea, 150 mM NaCl and 50 mM Tris-HCl) at 4 °C for 30 min. 23 mg of Fe₃O₄-MTX-Ni²⁺ was then added into the denaturant solution containing HBc₁₄₄-His subunits and vortexed at 4 °C for 10 min.

The reassembly of VLPs was initiated at 4 °C by dialyzing the dissociated HBc₁₄₄-His subunits in an assembling buffer A (50 mM Tris-HCl, pH 8.0, 150 mM NaCl, 10% v/v glycerol, 1% w/v glycine). After 12 h, the dialysate was replaced by assembling buffer B (50 mM Tris-HCl, pH 8.0, 150 mM NaCl, 1% w/v glycine) and dialyzing for another 12 h. The Fe₃O₄-MTX-Ni²⁺-containing VLPs (Fe₃O₄-MTX@HBc) were finally acquired by magnetic separation and lyophilization (-20 °C, 12 h).

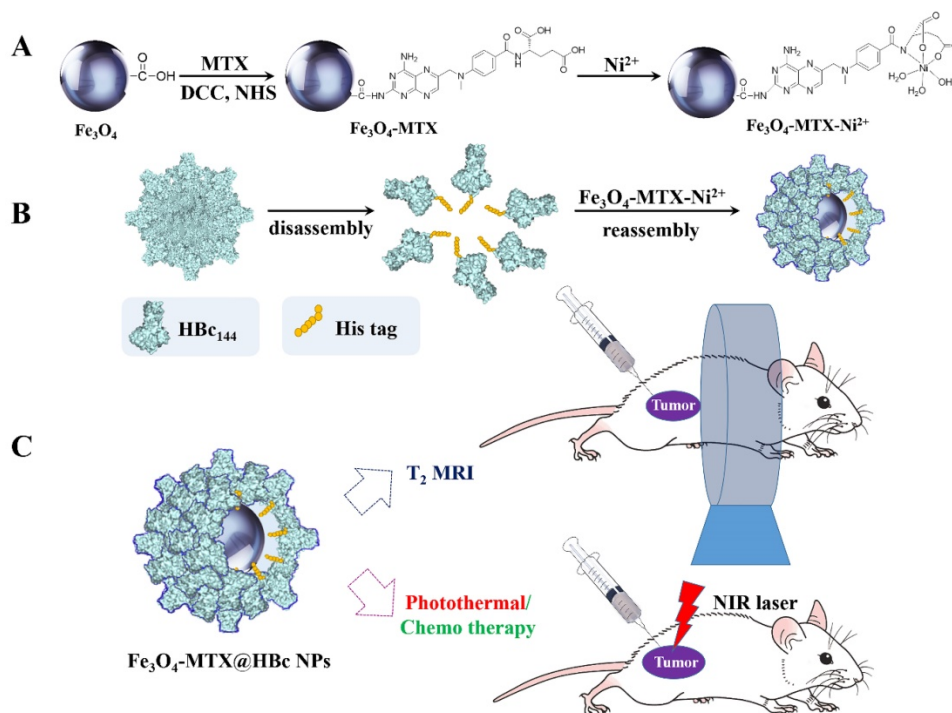
Characterization

The hydrodynamic radius of Fe₃O₄-MTX@HBc was determined by dynamic light scattering (DLS) measurements using Malvern Zetasizer Nano ZS (Malvern Instruments Ltd., Worcestershire, U.K.). Morphology and structure of the prepared NPs were characterized by a transmission electron microscopy (TEM, Tecnai G2 Spirit, FEI, USA) after the samples were negatively stained using 2 % TPA. Powder X-ray diffraction (XRD) patterns were collected using a German Bruker-axs D8-A25 X-ray diffractometer. The fourier transform infrared spectra (FT-IR) were recorded on a Fourier transform infrared spectroscope (Nicolet IS10, Thermo Fisher Scientific, USA). The drug loading efficiency of MTX in Fe₃O₄-MTX NPs was determined by high performance liquid chromatography (HPLC, separations module 2695, photo diode array detector 2996, Waters, USA). Photothermal experiments were conducted using an infrared reflector lamp (Hi-Tech optoelectronics, China) with a power density of 1.5 W·cm⁻². The

temperature and thermal images were collected by infrared thermal camera (FLIR A35, FLIR, Sweden). A vibration sample magnetometer (Lake Shore 7404, Lake shore, USA) was used to measure the magnetic properties of the as-prepared samples. The concentration of Fe³⁺ was determined by inductively coupled plasma mass spectrometry (ICP-MS, 7500 CE, Agilent, USA).

T₂-weighted MRI of Fe₃O₄-MTX@HBc

T₂-weighted MRI was measured by a 7.0 T Varian MRI system (Agilent Technologies, USA) with a horizontal-bore Magnex



Scheme 1. The detailed synthetic procedure and potential application for Fe₃O₄-MTX@HBc NPs.

magnet, equipped with 10 cm bore imaging gradients ($40 \text{ G}\cdot\text{cm}^{-1}$). Different concentrations of Fe in $\text{Fe}_3\text{O}_4\text{-MTX@HBc}$ (0.18, 0.37, 0.74, 1.48, and $2.97 \text{ mg}\cdot\text{mL}^{-1}$) were suspended in 0.1% agarose for MRI. The testing parameters were adopted: TR (repetition time) = 2000 ms, TE (echo time) = 60 ms, matrix size = 192×192 , slice thickness = 2 mm and FOV = 80×50 . By fitting the reciprocal of T_2 relaxation time (s^{-1}) against the concentration of Fe in a line, the r_2 relativity values were derived from the slope of the formula representing the line.

For *in vitro* T_2 -weighted MRI, 4T1 cells were incubated with culture media containing $\text{Fe}_3\text{O}_4\text{-MTX@HBc}$ ($200 \mu\text{g}\cdot\text{mL}^{-1}$) and equal amount of $\text{Fe}_3\text{O}_4\text{-MTX}$ NPs for 1 h, 2 h and 3 h, respectively. The cells were harvested and washed with PBS to remove the free NPs. Then 10^7 cells were suspended in 0.1% agarose for *in vitro* MRI. The testing parameters were adopted: TR = 2500 ms, TE = 11 ms, matrix size = 256×256 , slice thickness = 1 mm, and FOV = 40×40 .

In the T_2 -weighted MRI of tumors *in vivo*, the murine breast cancer 4T1 subcutaneous xenograft tumor bearing mice (tumor size: $\sim 400 \text{ mm}^3$) were used. The MRI were performed before and after 30 min post of the intratumoral injection of $\text{Fe}_3\text{O}_4\text{-MTX@HBc}$ ($100 \mu\text{L}$, 4 mg mL^{-1}). The transverse plane MR images were acquired using the following parameters: TR = 2000 ms, TE = 60 ms, matrix size = 128×128 , slice thickness = 2 mm, and FOV = 40×40 .

In Vitro Photothermal effect of $\text{Fe}_3\text{O}_4\text{-MTX@HBc}$ NPs

The murine breast cancer 4T1 cells were cultured in RPMI 1640 medium supplemented with 10% fetal bovine serum (FBS), 100 units $\cdot\text{mL}^{-1}$ penicillin and $0.1 \text{ mg}\cdot\text{mL}^{-1}$ streptomycin, at 37°C in 5% CO_2 . After 4 h of incubation with $\text{Fe}_3\text{O}_4\text{-MTX@HBc}$ NPs ($200 \mu\text{g}\cdot\text{mL}^{-1}$) or normal medium (control), the cells were collected in vials. The cell pellets were irradiated for 5 min with an 808 nm laser at a power of $2 \text{ W}\cdot\text{cm}^{-2}$ (facula 0.5 cm). The temperature and thermal images were collected with an infrared thermal camera (FLIR A35, FLIR, Sweden). After the cells were seeded in 96-well plates with 5000 cells/well and cultured for 12 h, $\text{Fe}_3\text{O}_4\text{-MTX@HBc}$ NPs with different concentrations ($25, 50, 100, 200,$ and $300 \mu\text{g}\cdot\text{mL}^{-1}$) were added to the wells, respectively. For photothermal treatments, the cells were treated with 5 min of irradiation of 808 nm laser light at power density ($2 \text{ W}\cdot\text{cm}^{-2}$, facula 1.5 cm). After the cells were incubated at 37°C for 24 h, $20 \mu\text{L}$ of MTT ($5 \text{ mg}\cdot\text{mL}^{-1}$ in PBS) was added into each well and incubated for another 4 h. The medium in each well was replaced by $200 \mu\text{L}$ of DMSO after the 4 h of incubation, and the plates were gently shaken for 0.5 h to dissolve the formazan precipitate. The cells were

followed by determining absorbance at 490 nm using a spectrophotometric microplate reader (Infinite 200 pro, Tecan, Switzerland).

4T1 cells were seeded in 12 well plates at 1×10^5 cells per well. After 12 h of incubation, $200 \mu\text{g}\cdot\text{mL}^{-1}$ of $\text{Fe}_3\text{O}_4\text{-MTX@HBc}$ NPs was added to cells for another 6 h of incubation before exposed to NIR laser (808 nm , $2 \text{ W}\cdot\text{cm}^{-2}$) for 5 min. Cells incubated with normal medium were used as control group. Annexin V-FITC/PI Apoptosis Detection Kit was used to analyze cell apoptosis by flow cytometry (BD Accun, Becton Dickinson Medical Devices, USA) after 12 h of incubation followed by the standard protocols.

In Vivo Biodistribution analysis of $\text{Fe}_3\text{O}_4\text{-MTX@HBc}$ NPs

For *in vivo* biodistribution analysis, $100 \mu\text{L}$ of $\text{Fe}_3\text{O}_4\text{-MTX@HBc}$ and $\text{Fe}_3\text{O}_4\text{-MTX}$ NPs (both amount of $12 \text{ mg}\cdot\text{kg}^{-1}$) were separately intratumorally injected into the murine breast cancer 4T1 subcutaneous xenograft tumor bearing mice (tumor size: $150\text{-}200 \text{ mm}^3$). The mice were sacrificed after 2 h of injection and the Fe^{3+} ions content of tissues (including heart, liver, spleen, lung, kidney, brain and tumors) were measured by inductively coupled plasma mass spectrometry (ICP-MS, 7500CE, Agilent, USA).

In Vivo Photothermal Therapy of tumor

The BALB/c mice were purchased from Beijing Vital River Laboratories Animal Technology Co. Ltd. and were taken care of under Institutional Animal Care and Use Committee of Xiamen University. 0.1 mL of 4T1 cell suspension (1×10^6) was subcutaneously injected to the mice (6 - 8 week). When the tumor size was up to $150 - 200 \text{ mm}^3$, the mice were intratumorally injected with or without $100 \mu\text{L}$ of $\text{Fe}_3\text{O}_4\text{-MTX@HBc}$ NPs ($12 \text{ mg}\cdot\text{kg}^{-1}$).

For *in vivo* PTT, the tumors were irradiated by 808 nm NIR laser ($1.5 \text{ W}\cdot\text{cm}^{-2}$, facula 1.0 cm) for 5 min. The real-time temperature and infrared thermal images of the tumor sites were recorded by an infrared thermal camera (FLIR A35, FLIR, Sweden).

For *in vivo* therapeutic efficacy, the growth rate of tumors was investigated by monitoring the tumor volumes (as calculated by the formula (1)) and body weight of mice per day.

$$V = a \times b^2 / 2 \quad (1)$$

Where a and b indicated the longest diameter and the shortest diameter, respectively. The tumors were photographed during the therapy period. The mice were euthanized on 10th day to detach the tissues (including heart, liver, spleen, lung, kidneys and tumors) and followed by further histological examinations using the hematoxylin and eosin (H&E) staining.

Results and Discussion

Preparation of Fe₃O₄-MTX NPs

To facilitate the efficient encapsulation in HBC₁₄₄-His VLPs, monodispersed Fe₃O₄ NPs with a size of 10 - 15 nm were prepared (Fig. S1A). XRD patterns demonstrated the successful synthesis of Fe₃O₄ (Fig. S1B). For combination of PTT with chemotherapy, MTX was conjugated to the surface of Fe₃O₄ NPs via the covalent attachment between MTX and DMSA functionalized Fe₃O₄ NPs. FT-IR spectra were collected to prove the existence of amido bond (Fig. S2A). The magnetic property of MTX modified Fe₃O₄ NPs was measured and then displayed by magnetic hysteresis loop (Fig. S2B). The measurement showed that Fe₃O₄-MTX NPs owned a saturation magnetization value (Ms) of 9.1 emu·g⁻¹. The drug loading efficiency of MTX in Fe₃O₄-MTX NPs was determined at 3.4%.

Preparation of Fe₃O₄-MTX@HBC NPs

In order to efficiently encapsulate the Fe₃O₄-MTX NPs into VLPs, HBC₁₄₄-His VLPs were engineered interiorly possessing histidine tags by genetic engineering to attract the Fe₃O₄-MTX-Ni²⁺ chelate during the process of encapsidation.²⁹ The HBC₁₄₄-His VLPs were obtained from *E.coli*. Sodium dodecyl sulfate polyacrylamide gel electrophoresis (SDS-PAGE) was performed to yield a single band corresponding to molecular weight of 14 kDa, indicating the corresponding molecular weight (14

KDa) of HBC₁₄₄-His subunit (Fig. 1A).

To increase the dispersibility and biocompatibility of Fe₃O₄-MTX NPs under biological conditions, monodispersed Fe₃O₄-MTX@HBC NPs were prepared by encapsulating Fe₃O₄-MTX NPs into HBC₁₄₄-His VLPs. Morphology of Fe₃O₄-MTX@HBC NPs was confirmed by TEM image (Fig. 1B). The shells were formed regularly by the composition of HBC₁₄₄-His units. The Fe₃O₄-MTX cores inside the NPs presented much darker color than the protein shells. The analogous core-shell structure of Fe₃O₄@HBC VLPs has been demonstrated by atom force microscopy (AFM) and magnetic force microscopy (MFM) in our previous work.²⁸ The encapsulation efficiency of Fe₃O₄-MTX@HBC₁₄₄-His NPs could reach 89 % through counting more than 200 NPs according to the large-scale TEM images. The hydrodynamic size of Fe₃O₄-MTX@HBC NPs was 38.2 ± 5.6 nm measured by DLS (Fig. 1B). Hence, the encapsulation of Fe₃O₄-MTX NPs into HBC₁₄₄-His VLPs could yield monodispersed, well-defined, hybrid nanostructures and facilitate addressable functionalization of the Fe₃O₄-MTX NPs.

The proportion of Fe₃O₄-MTX in Fe₃O₄-MTX@HBC NPs was determined by ICP-MS, indicating that there was 0.067 mg of Fe in 1 mg of Fe₃O₄-MTX@HBC NPs, based on which it was calculated that there were 13.8% Fe₃O₄-MTX and 86.2% other contents mainly protein in the Fe₃O₄-MTX@HBC NPs.

Photothermal effects

In order to confirm that Fe₃O₄-MTX@HBC NPs could be utilized as PTT agent, the photothermal performance was investigated. Fe₃O₄-MTX@HBC NPs in different concentrations were exposed to 808 nm NIR laser with power density of 1.5 W·cm⁻². When 0.1 mg mL⁻¹ of Fe₃O₄-MTX@HBC NPs were exposed to NIR laser, the temperature of the suspension had an increase of 20.2 °C in 5 min. Analogously, when the concentration of Fe₃O₄-MTX@HBC NPs reached to 0.2 and 0.4 mg mL⁻¹, the temperature of dispersions remarkably heightened by 27.5 °C and 33.3 °C, respectively. In comparison, the temperature of PBS as control did not change obviously in 5 min (Fig. 1C). Photothermal

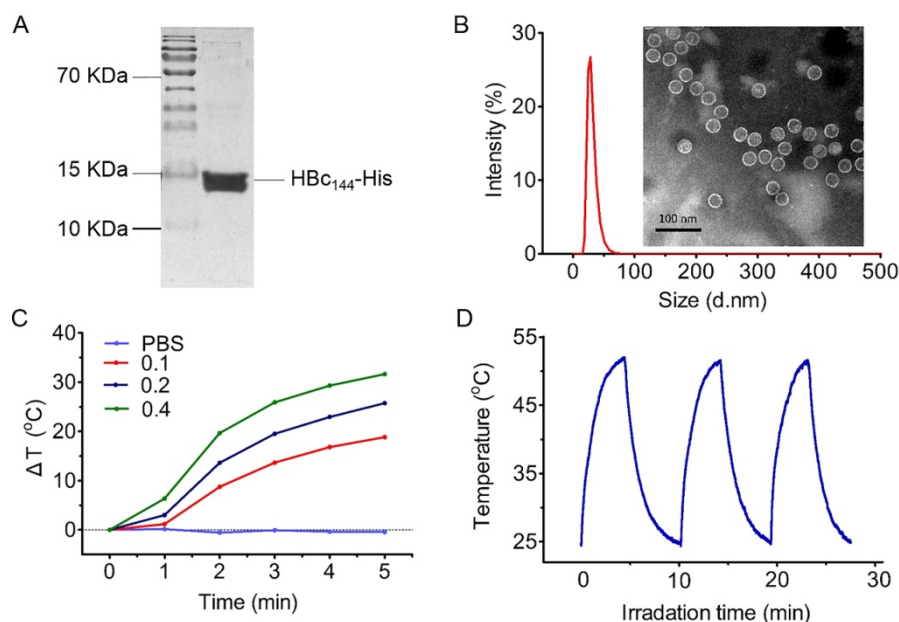


Figure 1. Characterization and photothermal effects of Fe₃O₄-MTX@HBC NPs: (A) SDS-PAGE image of HBC₁₄₄-His subunit; (B) Hydrodynamic size distribution and TEM image of Fe₃O₄-MTX@HBC; (C) Temperature increase of Fe₃O₄-MTX@HBC (0.1, 0.2, and 0.4 mg mL⁻¹) in PBS irradiated by 808 nm NIR laser at a power density of 1.5 W·cm⁻² (facula 0.5 cm); and (D) Photothermal stability of Fe₃O₄-MTX@HBC with NIR laser on and off for 3 cycles.

stability of Fe₃O₄-MTX@HBc NPs was also investigated by 5 min of continuous irradiation followed by another 5 min of irradiation after dropping to the room temperature for three cycles. It can be visualized from the curves that there was no obvious photothermal ability change happened in 3 cycles (Fig. 1D). After NIR laser irradiation, Fe₃O₄-MTX@HBc NPs still exhibited good dispersion in PBS, indicating that Fe₃O₄-MTX@HBc NPs have an excellent photothermal stability and great potential for use in thermal therapy.

In Vitro Photothermal-Chemo Therapy of Fe₃O₄-MTX@HBc NPs

To investigate the *in vitro* photothermal effect of Fe₃O₄-MTX@HBc NPs, 4T1 cells were treated by Fe₃O₄-MTX@HBc NPs and NIR laser. The thermal images of 4T1 cell pellet were shown in Fig. 2A and the curves of cell pellet temperature versus time were shown in Fig. 2B. The temperature for cells treated by Fe₃O₄-MTX@HBc NPs increased to 50.6 °C, which was much higher than that for untreated cells (36.1 °C). To evaluate and compare the *in vitro* photothermal-chemo cytotoxicity of Fe₃O₄-MTX@HBc NPs with or without NIR light irradiation, the viability of 4T1 cells was determined by MTT assay. Various concentrations of Fe₃O₄-MTX@HBc NPs were incubated with 4T1 cells for 24 h and treated with or without NIR light irradiation (808 nm, 2W·cm⁻² for 5 min). As in shown Fig. 2C, Fe₃O₄-MTX@HBc NPs exhibited cytotoxicity without NIR light irradiation

and all experiments evidenced an increasing cytotoxicity against 4T1 cells in a dose-dependent manner, revealing that the attachment of MTX to Fe₃O₄ NPs did not influence the chemo cytotoxicity of MTX. It presented a much higher efficacy of Fe₃O₄-MTX@HBc NPs to kill the tumor cells with 5 min of NIR irradiation, compared with the groups without light irradiation at all concentrations (Fig. 2C), indicating that Fe₃O₄-MTX@HBc NPs can effectively improve the efficiency of killing tumor cells *in vitro* by combining PTT and chemotherapy.

The cytotoxicity of Fe₃O₄-MTX@HBc NPs with NIR irradiation was verified by Annexin V-FITC/PI staining. Only untreated cells could not produce significant cell death. For the Fe₃O₄-MTX@HBc NPs groups, the cells with NIR irradiation exhibited significantly more apoptosis and necrosis (80.8%) than the cells without NIR irradiation (36.2%) (Fig. 2D). This result also confirmed the excellent synergistic effect of photothermal-chemo therapy of Fe₃O₄-MTX@HBc NPs.

T2-weighted MRI capability

As a noninvasive imaging tool, MRI is now widely used in hospitals for disease diagnosis, and can provide a three-dimensional anatomical image without exposing the body to ionizing radiation.³⁰ Fe₃O₄ NPs are commonly used as MRI contrast agents because they have the ability to shorten the T₂ relaxation time of surrounding water.³¹

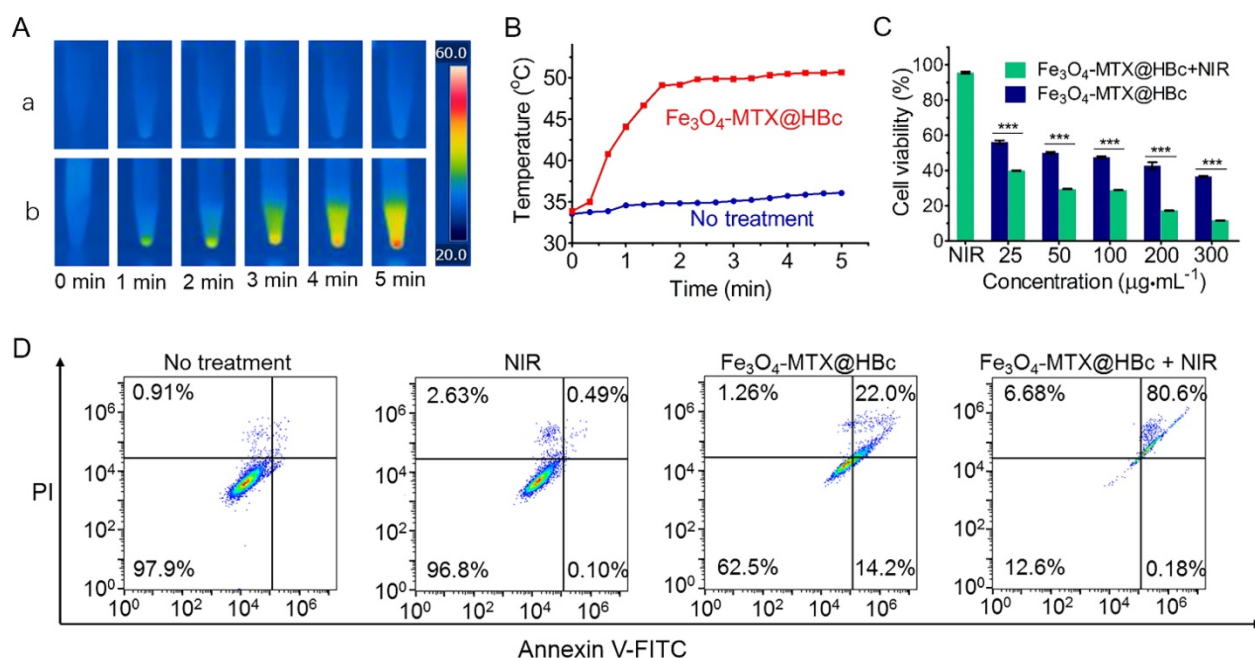


Figure 2. The *in vitro* PTT of Fe₃O₄-MTX@HBc NPs for 4T1 cells. (A) Thermal images of untreated 4T1 cells (a) and 4T1 cells incubated with Fe₃O₄-MTX@HBc NPs (b) under laser irradiation (2 W·cm⁻², facula 0.5 cm) for 5 min; (B) The curves of cell pellet temperature versus time during irradiation; (C) Cell viability of 4T1 cells incubated with different concentrations of Fe₃O₄-MTX@HBc NPs and irradiated with or without NIR light (n = 3, ***p < 0.001); (D) Flow cytometry plots for cellular apoptosis and necrosis after different treatments.

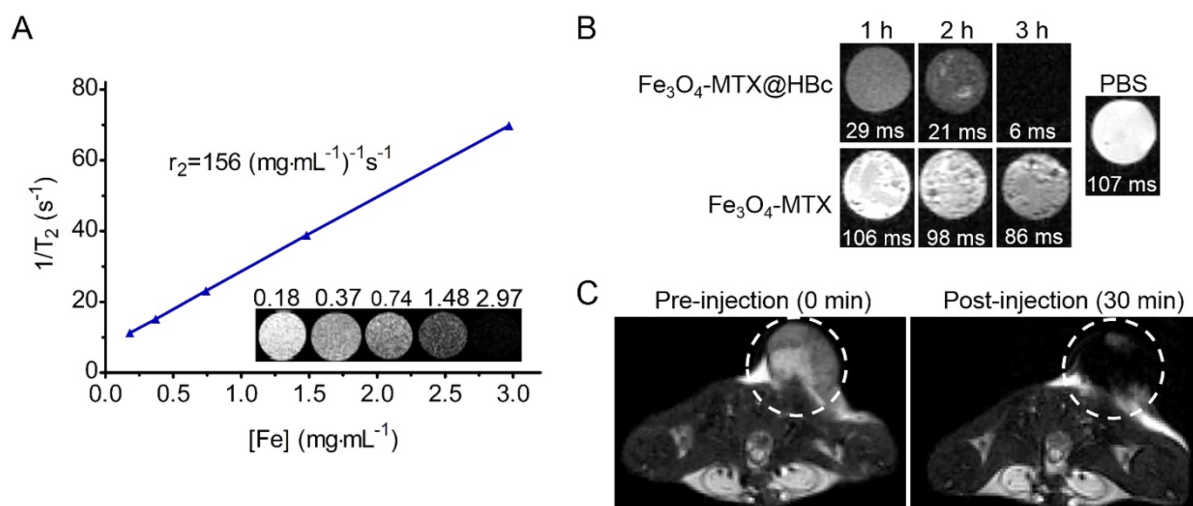


Figure 3. (A) Plot of spin-spin relaxation rate (T_2) against the concentration of $\text{Fe}_3\text{O}_4\text{-MTX@HBc}$ NPs and the T_2 weighted MRI for $\text{Fe}_3\text{O}_4\text{-MTX@HBc}$ NPs in different concentrations; (B) T_2 -weighted MRI of 4T1 cells after incubated with $\text{Fe}_3\text{O}_4\text{-MTX@HBc}$ and $\text{Fe}_3\text{O}_4\text{-MTX}$ NPs for 1 h, 2 h, and 3 h, respectively; (C) T_2 weighted MRI of 4T1 tumor bearing BALB/c mice before and after injection of $\text{Fe}_3\text{O}_4\text{-MTX@HBc}$ NPs for 30 min.

To measure the T_2 -weighted MRI ability of $\text{Fe}_3\text{O}_4\text{-MTX@HBc}$ NPs, the MRI of the NPs were performed. It can be observed from Fig. 3A that the brightness of $\text{Fe}_3\text{O}_4\text{-MTX@HBc}$ suspensions were getting lower along with the increasing concentration in the T_2 -weighted MR images. In the meantime, the inverse relaxation time (T_2^{-1}) versus Fe concentration fitted line well and the r_2 relativity values was $156 (\text{mg}\cdot\text{mL}^{-1})^{-1} \text{ s}^{-1}$, indicating the potential of $\text{Fe}_3\text{O}_4\text{-MTX@HBc}$ NPs to be a good T_2 -weighted MRI contrast agent. This might be due to that HBc VLPs could provide the advantages of proper size and shape, which can increase the chance of improving the rate of relaxation rates and the ideal modification of the contrast agent label.³²

In vitro T_2 -weighted MRI was performed to compare the cellular uptake efficiency of $\text{Fe}_3\text{O}_4\text{-MTX@HBc}$ and $\text{Fe}_3\text{O}_4\text{-MTX}$ NPs (Fig. 3B). Comparing with the $\text{Fe}_3\text{O}_4\text{-MTX}$ NPs treated group, the decrease of T_2 -weighted MR signal intensity and shorted T_2 relaxation time were obtained after cells incubating with $\text{Fe}_3\text{O}_4\text{-MTX@HBc}$ NPs for various durations. The results further demonstrated the higher cellular uptake efficiency of $\text{Fe}_3\text{O}_4\text{-MTX@HBc}$ over $\text{Fe}_3\text{O}_4\text{-MTX}$ NPs. This is due to that HBc₁₄₄-His VLPs are a kind of biocompatible protein materials and can improve the dispersion and stability of $\text{Fe}_3\text{O}_4\text{-MTX}$ under physiological conditions.

As the salient features of $\text{Fe}_3\text{O}_4\text{-MTX@HBc}$ NPs, the magnetism was further evaluated *in vivo* on T_2 -weighted MRI to afford guidance for cancer therapy. As shown in Fig. 3C, the clear tumor boundary and much darker interior could be observed after injected of $\text{Fe}_3\text{O}_4\text{-MTX@HBc}$ NPs. Which resulted from the decrease of T_2 -weighted MR

signal intensity at tumor sites. Such an obvious difference in T_2 -weighted signal could help to find the position of tumor precisely, even the position of high-density of cancer cells. These results demonstrated that $\text{Fe}_3\text{O}_4\text{-MTX@HBc}$ NPs could be used as a reliable MRI contrast agent for guiding therapy and reveal the *in vivo* biodistribution of themselves.

In Vivo Biodistribution analysis of $\text{Fe}_3\text{O}_4\text{-MTX@HBc}$ NPs

The *in vivo* biodistribution of $\text{Fe}_3\text{O}_4\text{-MTX@HBc}$ and $\text{Fe}_3\text{O}_4\text{-MTX}$ NPs were evaluated by the Fe^{3+} ions content in tissues and tumors. As shown in Fig. S3, after intratumoral injecting nanoparticles for 2 h in mice, the tumor accumulation of $\text{Fe}_3\text{O}_4\text{-MTX@HBc}$ NPs showed an enhancement of 1.39 folds than $\text{Fe}_3\text{O}_4\text{-MTX}$ NPs treated group. These results were attributed to that the presence of HBc₁₄₄-His VLP shell could increase the chemical stability and the dispersion of hydrophobic $\text{Fe}_3\text{O}_4\text{-MTX}$ under physiological conditions, as well as could also provide a protective layer for drug molecules and magnetite nanoparticles from the recognition by the reticuloendothelial system, therefore allowing drugs to be accumulated in the tumor over the prolonged periods of time.

The mice in $\text{Fe}_3\text{O}_4\text{-MTX@HBc}$ NPs treated groups (especially the one combined with PTT) exhibited remarkable delay in tumor growth or tumor regression compared to untreated group (Fig. 4C, D), demonstrating the outstanding photothermal-chemo synergistic effect of $\text{Fe}_3\text{O}_4\text{-MTX@HBc}$ NPs. No obvious weight changing was observed for all groups (Fig. 4E). All the mice were alive during the 10 days of therapy period.

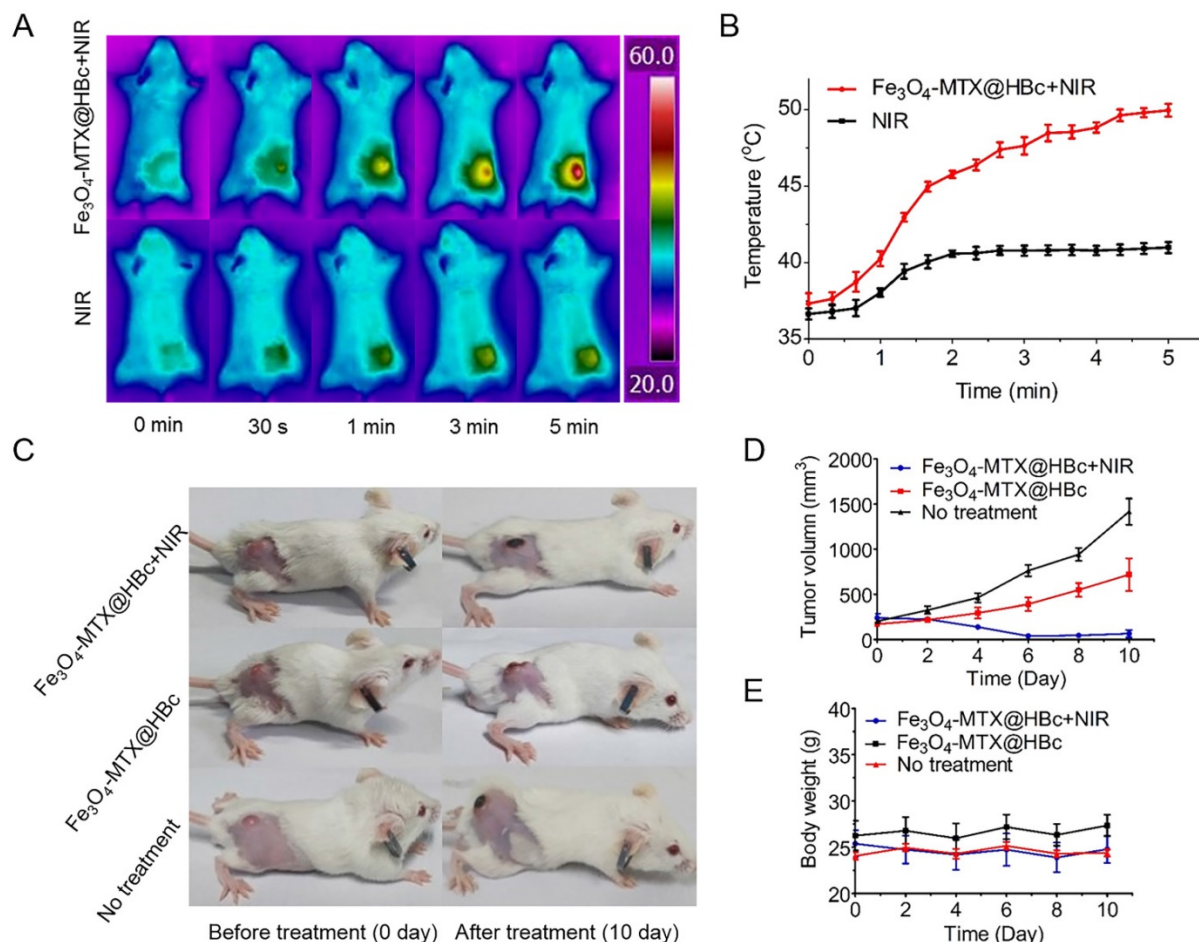


Figure 4. The PTT effect of Fe₃O₄-MTX@HBc *in vivo*. (A) Images and (B) the temperature curves of the tumor-bearing mice injected with or without Fe₃O₄-MTX@HBc under irradiation of 808 nm laser (1.5 W·cm⁻², facula 1.0 cm); (C) Photos of the tumor-bearing mice, (D) change of body weight and (E) tumor volume for different treated groups during therapy period.

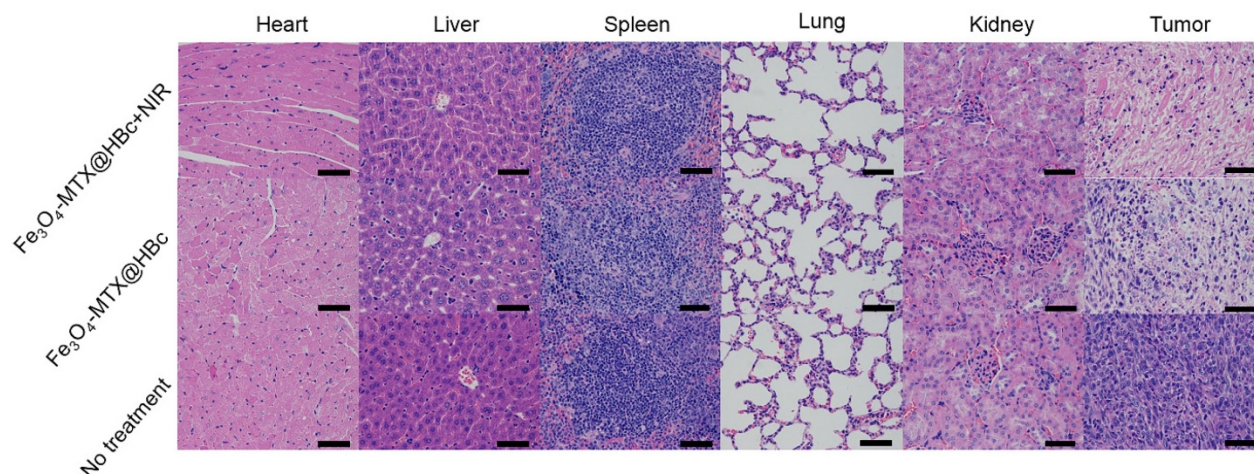


Figure 5. H&E stained images of tissues including heart, liver, spleen, lung, kidney and tumor after therapy. The scale bar is 100 μ m.

In vivo toxicity of Fe₃O₄-MTX@HBc NPs was analyzed by H&E staining and no obvious organ damages or toxic side effects were discovered in all groups, meanwhile the apparent coagulative necrosis

extensively existed in tumors in the mice of Fe₃O₄-MTX@HBc NPs treated groups (Fig. 5). All the results indicated that Fe₃O₄-MTX@HBc NPs had strong antitumour effect in the photothermal-chemo

synergistic treatment process *in vivo* and could be used as remarkable nanotheranostic agent for further biomedical researches and applications.

Conclusions

In this work, we developed a novel kind of multifunctional core-shell nanoparticles, which encapsulated Fe₃O₄-MTX NPs in HBC₁₄₄-His VLPs for MRI-guided photothermal-chemo therapy of cancer. The designed Fe₃O₄-MTX@HBC NPs possess good monodispersity, well-defined morphology, high r_2 relaxivity, good biocompatibility/biodegradation and strong NIR absorption feature. The outstanding MRI ability of Fe₃O₄-MTX@HBC NPs was confirmed on animals and visualized explicit effect of tumor magnetic resonance imaging. The therapeutic results of animal experiments reveal that the Fe₃O₄-MTX@HBC NPs present remarkable antitumor effect in combination of PTT and chemotherapy on cancer study. These excellent properties afford its applications as a theranostic nanoprobe for MRI-guided photothermal-chemo therapy of cancer.

Supplementary Material

Supplementary figures.

<http://www.ntno.org/v02p0087s1.pdf>

Acknowledgements

This work was supported by National Science Foundation of China (U1505228, 31371012), and Science Foundation of Fujian Province (2017Y0078).

Competing Interests

The authors have declared that no competing interest exists.

References

- Li L, Takemura G, Li Y, Miyata S, Esaki M, Okada H, et al. Preventive effect of erythropoietin on cardiac dysfunction in doxorubicin-induced cardiomyopathy. *Circulation*. 2006; 113: 535-43.
- Chiappinelli KB, Zahnow CA, Ahuja N, Baylin SB. Combining Epigenetic and Immunotherapy to Combat Cancer. *Cancer Research*. 2016; 76: 1683-9.
- Peiris PM, Abramowski A, McGinnity J, Doolittle E, Toy R, Gopalakrishnan R, et al. Treatment of Invasive Brain Tumors Using a Chain-like Nanoparticle. *Cancer Research*. 2015; 75: 1356-65.
- Robinson JT, Tabakman SM, Liang Y, Wang H, Casalongue HS, Vinh D, et al. Ultrasmall reduced graphene oxide with high near-infrared absorbance for photothermal therapy. *Journal of the American Chemical Society*. 2011; 133: 6825-31.
- Huang X, Elsayed IH, Qian W, Elsayed MA. Cancer cell imaging and photothermal therapy in the near-infrared region by using gold nanorods. *Journal of the American Chemical Society*. 2006; 128: 2115-20.
- Wang S, Riedinger A, Li H, Fu C, Liu H, Li L, et al. Plasmonic Copper Sulfide Nanocrystals Exhibiting Near Infrared Photothermal and Photodynamic Therapeutic Effects. *ACS Nano*. 2015; 9: 1788-800.
- Zheng M, Yue C, Ma Y, Gong P, Zhao P, Zheng C, et al. Single-Step Assembly of DOX/ICG Loaded Lipid-Polymer Nanoparticles for Highly Effective Chemo-photothermal Combination Therapy. *ACS Nano*. 2013; 7: 2056-67.
- Gallo J, Long NJ, Aboagye EO. Magnetic nanoparticles as contrast agents in the diagnosis and treatment of cancer. *Chemical Society Reviews*. 2013; 42: 7816-33.
- Jiang S, Eltoukhy AA, Love KT, Langer R, Anderson DG. Lipidoid-coated Iron Oxide Nanoparticles for Efficient DNA and siRNA delivery. *Nano Letters*. 2013; 13: 1059-64.

- Shen S, Kong F, Guo X, Wu L, Shen H, Xie M, et al. CMCTS stabilized Fe₃O₄ particles with extremely low toxicity as highly efficient near-infrared photothermal agents for *in vivo* tumor ablation. *Nanoscale*. 2013; 5: 8056-66.
- Li P, Chevallier P, Ramrup P, Biswas D, Vuckovich D, Fortin MA, et al. Mussel-Inspired Multidentate Block Copolymer to Stabilize Ultrasmall Superparamagnetic Fe₃O₄ for Magnetic Resonance Imaging Contrast Enhancement and Excellent Colloidal Stability. *Chemistry of Materials*. 2015; 27: 7100-9.
- Guo J, Yang W, Wang C. Magnetic colloidal supraparticles: design, fabrication and biomedical applications. *Advanced Materials*. 2013; 25: 5196-214.
- Zheng R, Wang S, Tian Y, Jiang X, Fu D, Shen S, et al. Polydopamine-Coated Magnetic Composite Particles with an Enhanced Photothermal Effect. *ACS Applied Materials & Interfaces*. 2015; 7: 15876-84.
- Shao D, Xu K, Song X, Hu J, Yang W, Wang C. Effective adsorption and separation of lysozyme with PAA-modified Fe₃O₄@silica core/shell microspheres. *Journal of Colloid & Interface Science*. 2009; 336: 526-32.
- Stamopoulos D, Gogola V, Manios E, Gourni E, Benaki D, Niarchos D, et al. Biocompatibility and Solubility of Fe₃O₄-BSA Conjugates with Human Blood. *Current Nanoscience*. 2009; 5: 177-81.
- Zhao Q, Chen W, Chen Y, Zhang L, Zhang J, Zhang Z. Self-assembled virus-like particles from rotavirus structural protein VP6 for targeted drug delivery. *Bioconjugate Chemistry*. 2011; 22: 346-52.
- Chen LS, Wang M, Ou WC, Fung CY, Chen PL, Chang CF, et al. Efficient gene transfer using the human JC virus-like particle that inhibits human colon adenocarcinoma growth in a nude mouse model. *Gene Therapy*. 2010; 17: 1033-41.
- Pokorski JK, Steinmetz NF. The art of engineering viral nanoparticles. *Molecular Pharmaceutics*. 2011; 8: 29-43.
- Yamada T, Iwasaki Y, Tada H, Iwabuki H, Chuah MK, Vandendriessche T, et al. Nanoparticles for the delivery of genes and drugs to human hepatocytes. *Nature Biotechnology*. 2003; 21: 885-90.
- Zhang Y, Ke X, Zheng Z, Zhang C, Zhang Z, Zhang F, et al. Encapsulating quantum dots into enveloped virus in living cells for tracking virus infection. *ACS Nano*. 2013; 7: 3896-904.
- Fang P Y, Holguin S Y, Hsiao C, et al. Functional RNAs: combined assembly and packaging in VLPs. *Nucleic Acids Research*. 2017; 45: 3519-27.
- Li C, Li F, Zhang Y, et al. Real-Time Monitoring Surface Chemistry-Dependent *In Vivo* Behaviors of Protein Nanocages via Encapsulating an NIR-II Ag₂S Quantum Dot. *ACS Nano*. 2015; 9: 12255-63.
- Pumpens P, Grens E. Hepatitis B core particles as a universal display model: a structure-function basis for development. *FEBS Letters*. 1999; 442: 1-6.
- Whitacre DC, Lee BO, Milich DR. Use of hepadnavirus core proteins as vaccine platforms. *Expert Review of Vaccines*. 2009; 8: 1565-73.
- Edman JC, Hallewell RA, Valenzuela P, Goodman HM, Rutter WJ. Synthesis of hepatitis B surface and core antigens in *E. coli*. *Nature*. 1981; 291: 503-6.
- Pumpens P, Borisova G P, Crowther R A, et al. Hepatitis B virus core particles as epitope carriers. *Intervirology*. 1995; 38:63-74.
- Shen LH, Bao JF, Wang D, Wang YX, Chen ZW, Ren L, et al. One-step synthesis of monodisperse, water-soluble ultra-small Fe₃O₄ nanoparticles for potential bio-application. *Nanoscale*. 2013; 5: 2133-41.
- Shen L, Zhou J, Wang Y, Kang N, Ke X, Bi S, et al. Efficient encapsulation of Fe₃O₄ nanoparticles into genetically engineered hepatitis B core virus-like particles through a specific interaction for potential bioapplications. *Small*. 2015; 11: 1190-6.
- Bharali DJ, Lucey DW, Jayakumar H, And HEP, Prasad PN. Folate-Receptor-Mediated Delivery of InP Quantum Dots for Bioimaging Using Confocal and Two-Photon Microscopy. *Journal of the American Chemical Society*. 2005; 127: 11364-71.
- Hu HH, Li Z, Pokorney AL, Chia JM, Stefani N, Pipe JG, et al. Assessment of cerebral blood perfusion reserve with acetazolamide using 3D spiral ASL MRI: Preliminary experience in pediatric patients. *Magnetic Resonance Imaging*. 2017; 35: 132-40.
- Liu B, Zhang X, Li C, He F, Chen Y, Huang S, et al. Magnetically targeted delivery of DOX loaded Cu₂S@mSiO₂@Fe₃O₄-PEG nanocomposites for combined MR imaging and chemo/photothermal synergistic therapy. *Nanoscale*. 2016; 8: 12560-9.
- Qazi S, Liepold LO, Abedin MJ, Johnson B, Prevelige P, Frank JA, et al. P22 Viral Capsids as Nanocomposite High-Relaxivity MRI Contrast Agents. *Molecular Pharmaceutics*. 2013; 10: 11-7.